

BRUSHLET SEGMENTATION FOR AUTOMATIC DETECTION OF LUMEN BORDERS IN IVUS IMAGES: A COMPARISON STUDY

Amin Katouzian¹, Elsa D. Angelini³, Bernhard Sturm⁴, Andrew F. Laine^{1,2}

Departments of ¹Biomedical Engineering, and ²Radiology, Columbia University, New York, USA

³Institut Telecom, Telecom ParisTech, CNRS LTCI, Paris, France

⁴Volcano Corporation, Rancho Cordova, CA USA

ABSTRACT

Due to high scattering effects inside lumen, detection of luminal borders in intravascular ultrasound (IVUS) images becomes challenging when high frequency transducers are employed. In this paper, we further study previously developed three-dimensional (3D) multiscale overcomplete brushlet-driven harmonic analysis, motivated by what experts visually do, to trace the lumen borders by exploiting spatial frame incoherence within blood speckle patterns. Two-dimensional (2D) brushlet coefficient clustering was designed to isolate blood pool and estimate the lumen borders with the surface function active (SFA) framework. We evaluated our proposed algorithm on phantom with flowing fluid and 1081 clinical IVUS images acquired from six patients with single-element 40 MHz and 45 MHz transducers. We quantified and compared the results with a threshold-based algorithm and a 2D shape-driven technique driven by non-parametric probabilistic energy functions. We highlight the advantages of each approach and discuss the robustness of proposed algorithm.

Index Terms— Brushlet, IVUS, Border Detection, Lumen, Multiscale analysis.

1. INTRODUCTION

In interventional radiology, the ultimate goal is to provide the cardiologists with reliable clinical tools to identify vulnerable plaques [1], choose the most appropriate drugs or implant devices (*i.e.* stent) to stabilize the plaques during catheterization procedures, with minimal risk. Intravascular ultrasound (IVUS) is a screening modality of particular interest to guide such intervention since it provides useful information about tissue microstructures and images with sufficient penetration as well as acceptable resolution.

Among morphological and structural markers associated with vulnerable plaques, thin cap fibroatheroma (TCFA $< 65\mu\text{m}$) is still not directly detectable due to inadequate spatial resolution ($> 100\mu\text{m}$), but inferable, from IVUS images. Newly developed high-frequency IVUS transducers are now being used to prevail this limitation and obtain rich spatiotemporal IVUS image data. As a drawback, detection of lumen borders becomes more challenging due to high scattering effects of red blood cells inside the lumen, which

makes blood-tissue interface less contrasted, as illustrated in **Figure 1**.

To tackle the segmentation problem, researchers have developed several algorithms, employing different techniques such as edge tracking and gradient-based techniques [2] active contours [3], statistical- and probabilistic-based methods [4-6], and multiscale approaches [7]. For example, Taki *et al.* [6] employed an affine invariant anisotropic filter for despeckling and enhancing borders and used two different threshold values to detect both vessel wall and lumen borders. Alternatively, Unal *et. al* [5] presented a 2D algorithm, implemented in the polar domain, which built a statistical shape space through principle component analysis (PCA). Once the shape space was built, an initialized contour evolved from the surface of the transducer (catheter marker) in polar coordinates by minimization of a region-based non-parametric probabilistic energy function. They estimated the probability distribution inside and outside the lumen using intensity profiles and constructed a training dataset to delineate the lumen borders automatically.

Despite the large amount of segmentation methods having been proposed, clinical applications of automated segmentation methods have seen limited success due to intrinsic challenges (presence of a guide wire, of calcified plaque, of side branches, motion of the catheter and the heart) and extrinsic challenges (IVUS system parameter specifications such as time gain compensation, compression of the vessel wall) associated with IVUS data acquisition setup. For example, variability among IVUS system specifications or change of acquisition parameters by experts would lead to inconsistency among data sets so that supervised techniques, knowledge based methods [2], or those that rely on statistical models of gray level intensities [5,6] may not perform efficiently.

The proposed method tackles these limitations by exploiting frequency-based harmonic information, via brushlet expansion. It is based upon a previously developed algorithm [12], which showed that tissue-specific backscattered magnitude and phase information, contained in brushlet coefficients, could discriminate different tissues on US images. This property was used to establish a framework able to generate binary masks corresponding to blood and non-blood regions, which ultimately made lumen

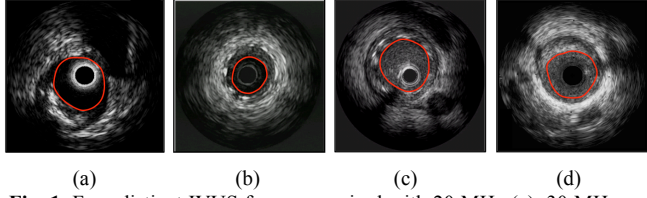


Fig. 1. Four distinct IVUS frames acquired with 20 MHz (a), 30 MHz (b), 40 MHz (c), and 45 MHz (d) transducers. Red contours represent lumen borders.

borders regularization easier. Unlike existing techniques, our proposed algorithm relies on directional sensitive spectral features and does not require any parameter tuning, specific initialization, or manual annotation. The proposed segmentation method also exploits surface function actives (SFA) [8] to finely detect lumen borders with specific geometric constraints. Segmentation results are compared to two existing state of the art segmentation techniques.

2. METHODOLOGY

2.1. Rational for harmonic analysis of US images

Interventional cardiologists often go back and forth among consecutive IVUS frames to visually locate the lumen border on a single frame. By doing so, blood speckle and plaque respectively embody visually incoherent and coherent spatial textural patterns, suggesting 3-D harmonic analysis to discriminate these two tissues. Brushlet analysis enables to perform spatially-localized harmonic expansion of images. Clustering of brushlet coefficients enables to discern the textural patterns corresponding to blood and non-blood regions. One of the major advantages of expansion of IVUS sub-volumes onto brushlet basis functions is that it is invariant to intensity, depending only on the frequency content of the IVUS signals. In addition, the brushlet expansion provides an orthogonal transform of the Fourier domain, which is Hermitian-symmetric (enabling separate manipulation of individual coefficients and reduction of the analysis dimension space by one half). We show in this work that the phase as well as the magnitude information of brushlet coefficients can be used to discriminate tissues in IVUS images and eventually to detect lumen borders.

2.2. Overview of brushlet expansion

The main advantage of brushlet analysis [9] functions over wavelet packets, steerable filters, and directionally oriented filter banks, is their computational efficiency and unique representation of features in Fourier space along with arbitrary tiling. More specifically, rich angular resolution is obtained through brushlet analysis by expansion of the Fourier transform (FT) space onto windowed Fourier bases. Given any one-dimensional signal $f \in L^2(R)$, its Fourier transform \hat{f} can be projected onto brushlet basis as:

$$\hat{f} = \sum_n \sum_j \lambda_{n,j} u_{n,j} \quad (1)$$

where $\lambda_{n,j}$ and $u_{n,j}$ represent brushlet coefficients and basis functions, respectively [9]. The parameters n and j encode respectively the subintervals of the frequency domain (of size l_n) and the index of the frequencies being analyzed, centered on this interval and on its extremities. By doing so, the FT of the signal is divided into subintervals. Each interval, indexed by n , and of size l_n is projected onto $u_{n,j}$, with $j=0, 1/l_n, \dots, (l_n-1)/l$. Full details on the implementation of the decomposition can be found in [10]. It has been shown that the projection of \hat{f} onto the brushlet basis can be implemented in an efficient fashion using a folding technique and fast Fourier transform (FFT) [9]. Separable tensor products of 1D basis functions are used to expand sub-volumes of IVUS images onto 3D brushlet bases. In **Figure 2**, we illustrate the schematic of the proposed brushlet extraction procedure, and the selection of features, from brushlet coefficients, along an arbitrary number of directions, encoded by positions of the centers of the cube.

2.3. Brushlet-based lumen border segmentation framework

Working on radial line measurements of an IVUS transducer during pullback, we rely on the assumption that the blood speckle pattern can be discriminated from the structural patterns of tissue layers, with homogeneous echogeneity, in the spectral Fourier domain. We speculate that in radial IVUS images, organized in textured layers of blood and tissues, different tissue echogeneities arise and scattering properties can be encoded in the brushlet coefficient magnitudes. We also speculate that blood and non-blood tissues generate backscattered signals with different incoherence, encoded in the phase of the brushlet coefficients. We therefore hypothesize that the magnitudes and phases of brushlet coefficients provide discriminative features for high-echogeneity and coherent (non-blood) versus low-echogeneity and incoherent (blood) patterns so that we can estimate the lumen border in the transformed domain via selection of specific clusters of phases-magnitudes combinations. Such approach is superior to simple magnitude coefficient thresholding for selective reconstruction of tissue layers.

The proposed method takes advantages of properties associated with brushlet expansion to establish a segmentation framework by clustering coefficients corresponding to blood and non-blood regions. First, we know that blood speckle resembles noise-like patterns within contingent sets of IVUS frames, which correspond to high frequency components localized in the outermost cubes of the brushlet space. Secondly, brushlet expansion is performed with overcomplete representations to guarantee a bi-jection within and among each expansion sub-volumes

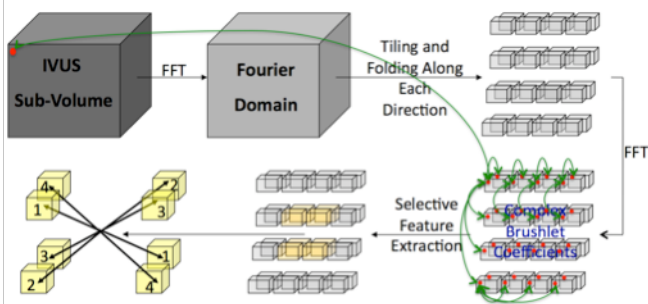


Fig. 2. Schematic expansion of IVUS sub-volumes onto brushlet basis functions, tiling the frequency domain with $(4 \times 4 \times 2)$ blocks and performing selective feature extraction along eight directions corresponding to low-frequency components. Bi-jection within and among each expansion sub-volume and a one-to-one correspondence of the coefficients across sub-spaces of the expansion are illustrated by the green arrows for individual pixels within and across sub-volumes.

and a one-to-one correspondence of the coefficients across sub-spaces of the expansion, as illustrated in **Figure 2**. Moreover, there is a homomorphism between the original domain of acquisition (*i.e.* spatial domain) and the brushlet space (*i.e.* unique correspondence between IVUS voxels and brushlet coefficients). This allows us to construct joint magnitude-phase histograms of summed coefficients in the innermost cubes that represent low frequency components and retain the most informative spatial features corresponding to each peak as illustrated in **Figures 3**. From joint magnitude-phase histograms of coefficients, we identify clusters of magnitude-phase joint values that are used to generate binary masks corresponding to each regional peak of the joint-histogram as described in [12,13]. Thirdly, spatial regularization of the binary mask with Markovian constraints is performed prior to the detection of the lumen border with the SFA framework [9] manipulating 1D sine and cosine shape bases as follows:

$$g(a_k, b_k, \theta) = a_0 / 2 + \sum_{k=1}^M \left(a_k \cos\left(\frac{2k\pi\theta}{N_\theta}\right) + b_k \sin\left(\frac{2k\pi\theta}{N_\theta}\right) \right) \quad (2)$$

where N_θ is number of angles that span 360° in Cartesian space or the width (x) of the image in polar coordinates. The height (y) of the polar mask-images encodes the radial position of the lumen border. The weight coefficients (a_k, b_k) are optimized through an iterative process so that the SFA function $g(a_k, b_k, \theta)$ converges to 0.

3. RESULTS

We processed IVUS sub-volumes of size $512 \times 512 \times 8$ voxels to ensure adequate spatial resolution in the pullback direction (*i.e.* 8 slices depth). Longer depth degraded the performance of the brushlet coefficient clustering due to the effects of the motion of the catheter and the heart. The Fourier domain was tiled using $(4 \times 4 \times 2)$ cubes in (x, y, z) directions (z = pullback direction). In this case, the brushstroke orientation was degrees in the (x, y, z) directions.

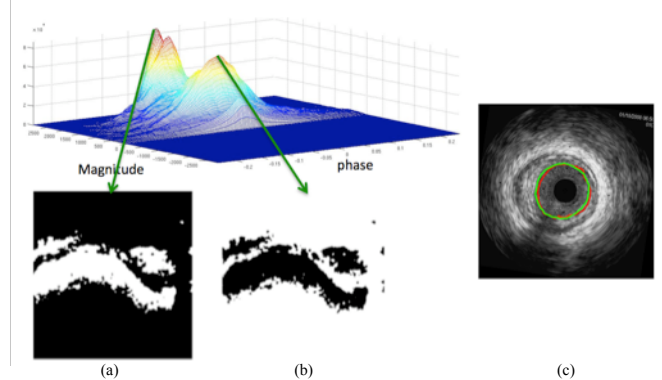


Fig. 3. Constructed 2.5-D magnitude-phase histogram (top), generated binary masks corresponding to individual histogram peaks (a,b), detected lumen border (red) imposed on the IVUS grayscale image (c) along with manual traced border (green) by expert.

Previously, we investigated the feasibility of proposed technique, employing IVUS data acquired from a phantom cylinder made of shrink-wrap material with circulating blood-mimicking fluid [12]. We demonstrated that the histogram exhibited three peaks corresponding to coherent (cylinder wall material and the background) and incoherent (fluid) patterns. This experiment confirmed the ability of joint magnitude-phase clustering of brushlet coefficients to discriminate between a flowing fluid and a scattering material.

In this study, we evaluate the proposed clustering and segmentation algorithm performance on 1081 IVUS frames acquired from six patients during catheterization procedure employing single-element 40MHz and 45 MHz transducers. As shown in **Figure 3**, the joint histogram peaks were not as well separated as in the case of the phantom data [12] but they still provided good estimates of relative magnitudes and phases for blood and non-blood regions, enabling detection of lumen borders.

Performance of our proposed segmentation framework (*Method 1*) was compared with two existing techniques [5,6]: Unal *et. al* [5] (*Method 2*) who proposed a 2D segmentation method implemented in the polar domain, building a statistical shape model via principle component analysis (PCA). The position of the shape model is optimized by minimization of a region-based non-parametric probabilistic energy function. They estimated the probability distribution function (pdf) inside and outside the lumen area using intensity profiles learned on a training dataset. A second method from Taki *et. al* (*Method 3*) [6] was tested, preprocessing the IVUS images using affine-invariant anisotropic filtering in combination with hard thresholding and employing a geometric deformable model to estimate the lumen border. Results from the *Method 3*, illustrated in **Figure 4**, revealed that a unique threshold value was not well suited for all IVUS cases so that we had to rely on an empirical selection of the thresholds on individual cases to achieve optimal segmentation performance. We can also see that the separation between the histograms of the inside and outside regions vanishes as the transducer center frequency increases from 20MHz to

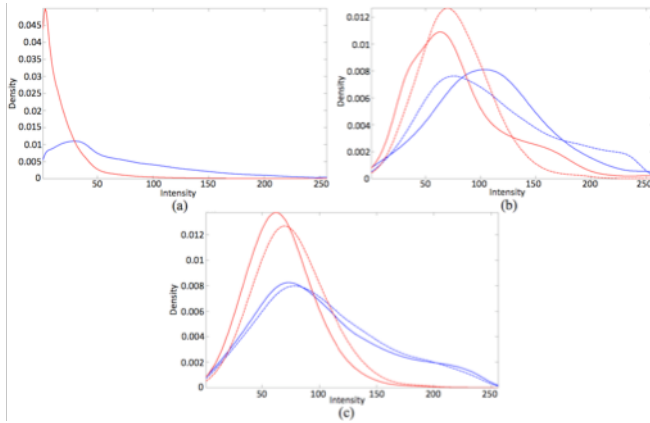


Fig. 4. Probability density distribution inside (red) and outside (blue) derived from images acquired with 20 MHz (a), 40 MHz (b), and 45 MHz (c) transducers. The probability distributions were computed from two datasets (solid and dashed lines) in images acquired with 40 MHz and 45 MHz transducers.

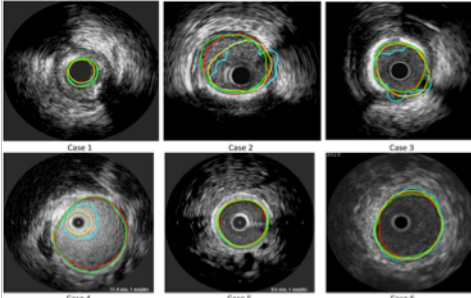


Fig. 5. Resulting automated lumen border detected in images acquired with 45MHz (top row) and 40 MHz (bottom row) single-element transducers with the proposed technique (red), Method 2 (yellow), and Method 3 (cyan), along with manually traced contours (green), collected from six *in vivo* cases.

45MHz, making segmentation more challenging for pdf- and threshold-based techniques.

Quantitative comparisons of lumen borders for all three methods over the six cases are reported in **Table 1**, with the following accuracy measures: true positive (TP), false positive (FP) overlaps, and root mean squared error (RMSE), comparing to manual tracing by an expert. **Figure 5** illustrates the automated detected lumen borders identified on six distinct IVUS images with our proposed technique (red), *Method 2* (yellow) and *Method 3* (cyan) along with manually traced borders (green) from an expert. From the results, we observe that the other two techniques completely failed in one case, which was correctly segmented with the proposed method. *Method 2* outperformed our proposed method in 2 cases for TP/FP measures but not for RMSE measures. Overall, the proposed method ranked the 1st on 4 over 6 cases.

5. CONCLUSION

This paper describes a novel technique, based on harmonic analysis of polar IVUS images, acquired with 40MHz and 45MHz transducers, to cluster brushlet coefficients and reliably detect lumen borders. The proposed technique, was evaluated on a reasonable number of *in vivo* collected

Table 1. Quantification of automated lumen borders detection with three different methods compared to manually traced borders. The 1st, 2nd, and 3rd ranked methods are highlighted in green, orange, and red colors, respectively.

	TP(%)	FP(%)	RMSE (mm)		TP(%)	FP(%)	RMSE (mm)
Case 1				Case 4	97.8±0.03	4.4±0.06	0.040±0.081
Method 1	96.7±0.05	3.9±0.01	0.010±0.025	Method 1	51.2±0.00	0.00±0.0	0.980±0.121
Method 2	97.6±0.90	38.7±4.5	0.114±1.300	Method 2	58.1±0.10	0.07±0.0	0.231±0.206
Method 3	93.9±0.10	2.4±0.00	0.025±0.039	Method 3			
Case 2				Case 5	95.2±0.24	0.12±0.0	0.020±0.010
Method 1	91.1±1.00	5.0±0.20	0.030±0.129	Method 1	92.3±0.00	2.70±0.0	0.040±0.024
Method 2	83.8±0.40	5.1±0.20	0.104±0.946	Method 2	97.8±0.02	0.2±0.06	0.015±0.078
Method 3	80.8±0.05	9.0±0.20	0.130±0.982	Method 3			
Case 3				Case 6	92.8±0.43	0.50±0.00	0.040±0.054
Method 1	89.5±0.03	4.7±0.10	0.040±0.195	Method 1	94.8±0.09	0.12±0.03	0.023±0.016
Method 2	80.3±1.80	8.3±0.21	0.145±0.328	Method 2	99.9±0.06	3.70±0.03	0.025±0.023
Method 3	73.1±1.50	5.6±0.20	0.166±1.674	Method 3			

images (1081 frames from 6 cases). It outperformed two other state of the art methods, based on pdf intensity modeling or intensity thresholding. The thresholding method was parameterized empirically for each individual case, to optimize its performance versus the use of a single fixed threshold. One of the main challenge with IVUS images is that the appearance of images may vary depending on the selected parameters during acquisition (*e.g.* due to TGC manipulation), normalization/saturation, or reconstruction (*i.e.* non-linear transformation). This leads to variations among intensity profiles, which seem to increase with transducer frequency, and are only robust to spectral analysis, which is the main advantages of our proposed framework.

REFERENCES

- [1] E. Falk, "Why do plaques rupture?", *Circulation*, Vol. 86, pp. III30-III42, 1992.
- [2] M. Sonka, X. Zhang, M. Siebes, M. S. Bissing, S. C. DeJong, S. M. Collins, C. R. McKay, "Segmentation of Intravascular Ultrasound Images: A Knowledge-Based Approach," *IEEE Tran. Med. Imag.*, vol. 14, no. 4, pp. 719-732, Dec. 1995.
- [3] G. Kovalski, R. Beyar, R. Shoffi, and H. Azhari, "Three-dimensional automatic quantitative analysis of intravascular ultrasound images," *Ultrasound in Medicine and Biology*, vol. 26, no. 4, pp. 527-537, 2000.
- [4] M. H. R. Cardinal, J. Meunier, G. Soulez, R. L. Maurice, E. Therasse, G. Cloutier, "Intravascular Ultrasound Image Segmentation: A Three-Dimensional Fast-Marching Method Based on Gray Level Distribution," *IEEE Tran. Med. Imag.*, vol. 25, no. 5, pp. 590-601, May 2006.
- [5] G. B. Unal, S. Bucher, S. Carlier, Gregory G. Slabaugh, Tong Fang, K. Tanaka, "Shape-Driven Segmentation of the Arterial Wall in Intravascular Ultrasound Images," *IEEE Tran. Info. Tech. Biomed.*, vol. 12, no. 3, pp. 335-347, 2008.
- [6] A. Taki, Z. Najafi, A. Roodaki, S. K. Setarehdan, R. A. Zoroofi, A. Konig, N. Navab, "Automatic segmentation of calcified plaques and vessel borders in IVUS images," *Int. J. CARS*, vol. 3, pp. 347-354, 2008.
- [7] A. Katouzian, B. Baseri, E. E. Konofagou, A. F. Laine, "Automatic Detection of Blood versus non-Blood Regions on Intravascular Ultrasound (IVUS) Images Using Wavelet Packet Signatures," in *Proc. SPIE Med. Imag.*, San Diego, Feb. 2008.
- [8] Q. Duan, E. D. Angelini, A. F. Laine, "Surface Function Actives," *J. Vis. Commun. Image R.*, Vol. 20, pp. 478-490, 2009.
- [9] F. Meyer and R. R. Coifman, "Brushlets: A tool for directional image analysis and image compression," *Applied and computational harmonic analysis*, vol. 4, pp. 147-187, 1997.
- [10] E. Angelini, A. Laine, S. Takuma, J. Holmes, S. Homma, "LV Volume Quantification via Spatio-Temporal Analysis of Real-Time 3D Echocardiography," *IEEE Trans. Med. Imag.*, Vol. 20, No. 6, pp. 457-469, 2001.
- [11] P. Ausher, G. Weiss, M. V. Wickerhauser, "Local sine and cosine bases of Coifman and Meyer and the construction of smooth wavelets," in *Wavelets- A tutorial in Theory and Application*, vol. 2, *Wavelet Analysis and its Applications*, C. K. Chui, Ed. San Diego: Academic Press, 1992, pp. 237-256.
- [12] A. Katouzian, E. Angelini, B. Sturm, A. F. Laine, "Automatic detection of luminal borders in IVUS images by magnitude-phase histograms of complex brushlet coefficients," *Conf. Proc. IEEE Eng. Med. Biol. Soc.*, pp. 3073-6, 2010.
- [13] O. Yilmaz and S. Rickard, "Blind Separation of Speech Mixtures via Time-Frequency Masking," *IEEE Transactions on Signal Processing*, Vol. 52, No. 7, pages 1830-1847, July 2004.